Exploration of the environments of nearby stars with the NICMOS coronagraph - instrumental performance considerations

Glenn Schneider[a], Rodger I. Thompson[a], Bradford A. Smith[b], and Richard J. Terrile[c]

[a] Steward Observatory, 933 N. Cherry Ave., University of Arizona, Tucson, AZ 85750
[b] Institute for Astronomy, Univ. of Hawaii, PO Box 4729, Hilo, HI 96720
[c] Jet Propulsion Laboratory, MS 183-501, Pasadena, CA 91109

ABSTRACT

The Near Infrared Camera and Multi-Object Spectrometer (NICMOS), installed into the Hubble Space Telescope (HST) in February 1997, incorporates a coronagraphic imaging capability. The coronagraph is comprised of two optical elements. The camera 2 field divider mirror, upon which the HST f/24 input beam is imaged, includes a 170µm diameter hole which contains ~93% of the encircled energy from a stellar Point Spread Function (PSF) at a wavelength of 1.6µm. The coronagraphic hole lowers both the diffracted energy in the surrounding region by reducing the high spatial frequency components of the occulted core of the PSF, and down stream scattering. The geometrical radius of this occulting spot, when re-imaged through the camera 2 f/45 optics, is ~4 pixels (or 0.3") at the detector focal plane. An oversized cold pupil-plane mask (maintained at ~100K), with radial structures co-aligned with the HST secondary mirror spider, acts over the whole 19.1"x19.2" field to further reduce the diffracted energy in the direction of the spider vanes. The absolute performance levels of the coronagraph were ascertained during the Servicing Mission Observatory Verification (SMOV) program. Using a differential imaging strategy (by rolling the spacecraft) we expect to achieve statistically significant detections of sub-stellar companions at 1.6µm with a ΔH of ~10 and separations as close as 0.5" (corresponding to 2.5AU at 5pc). The NICMOS Environments of Nearby Stars (EONS) programs is exploiting this capability in systematic surveys of nearby, and young stars searching for brown dwarfs and giant planets, and protoplanetary disks around main-sequence stars.

Keywords: Infrared, Coronagraphy, Hubble Space Telescope, Brown Dwarfs, Extra-Solar Planets

1. SCIENTIFIC MOTIVATION

The discovery and characterization of low mass, sub-luminous objects in stellar systems is one of the key goals of contemporary observational astronomy and astrophysics. From the low-mass end of the mass-luminosity function (which is very poorly constrained for $M_* \leq 0.2$ M(sun)) into the ≤ 0.08M(sun) regime of brown dwarfs and transitional objects, and down into the domain of giant planets, the near and sub-stellar bestiary remains fertile ground for fundamental exploration. Long before the recent adoption of NASA's *Origins* theme, which contains in it's foundation the establishment of scientific activities to investigate the birth and early evolution of stars and planets[1], the NICMOS Instrument Definition Team (IDT) embraced these goals in formulating our EONS program. A systematic search for previously unknown low-mass (giant planet and brown dwarf) companions to stars in the solar neighborhood, and circumstellar dusk disks around main sequence stars by direct coronagraphic imaging is a cornerstone of the EONS investigations.

A carefully selected candidate list of ~100 stars will be observed using the NICMOS coronagraph at 1.6µm. As demonstrated in the on-orbit SMOV test program, following the second HST servicing mission, we will be able to detect non-stellar companions as faint as H = 22, 10 to ~13 magnitudes fainter then their primaries at separations of 0.375" to ~3.0". For the stars in our sample this covers minimum physical separations of 1.2-50 AU at the inner spatial detection limit. The lower mass limit depends on age, distance, and spectral type, but can be as low as 3-5 M(Jupiter) for many of our targets. With such observations, we can address questions as fundamental as: Is there a continuity of objects across the sub-stellar mass spectrum bridging the main sequence to planetary objects? What is their frequency of occurrence? At what distances will they be found from their primaries? And, what implications will these discoveries have for our understanding of stellar/planetary formation mechanisms?

Contact: gschneider@as.arizona.edu, Telephone: 520-621-5865

1. THE EONS SEARCH AND CHARACTERIZATION PROGRAMS

The EONS search programs were designed to identify low-mass and sub-stellar companions over two decades in the mass-spectrum. Knowledge of stellar and sub-stellar masses and luminosities at and below the ≤0.08 M(sun) H-burning limit is of fundamental importance in many inter-related areas such as the determination of the stellar mass function at the lowest masses, the theory of stellar evolution, the study of the end of the main sequence, the search for galactic missing mass, the resolution of age/evolution issues and the origins of stellar and planetary systems. Yet, this transition region between low-mass stars and giant planets is poorly understood and ill-observed. Until recently, with the discovery and imaging of the brown dwarf companion to GL 229[2], the very existence of such objects remained in the conjectural realm. Continuing discoveries of companion objects to solar-like stars of 1-10 Jupiters and higher by *indirect* methods has revealed an unanticipated diversity in mass ranges, dynamical properties, and primary-star characteristics[3,4,5]. *Direct* observations of sub-stellar companions, including imaging, are required to characterize these newly-discovered objects and address the fundamental questions we have already raised.

To make further progress at the low end of the mass spectrum, additional objects must be found. The design of the NICMOS coronagraph allows probing the potentially fruitful hunting grounds in which to search for transitional objects and circumstellar disk material over parameter spaces which do not overlap with ground-based capabilities. Our EONS surveys, primarily, will obtain single-color coronagraphic images aimed at discovering such objects utilizing the 1.4-1.8μm H-band where the NICMOS coronagraphic performance is optimized. This wavelength band also corresponds to the strong emission in GL 229B[6] and GD 165B (as well as to strong reflections in Jupiter and Titan). Spatially, we concentrate in the astrophysically and dynamically interesting spatial regions of the search-space from 0.3" (the radius of the coronagraphic hole) to 3.0" (close to the edge of the field-of-view in one spatial direction).

Target selection for the EONS search programs was carefully considered and refined over a period of many years, and designed to maximize the probability of finding brown dwarf and giant planet companions, and circumstellar dust-disks, as appropriate to the parent stars. These selective surveys are being carried out as three separate programs under the NICMOS/HST Guaranteed Time Observing (GTO) utilizing ~18% of the IDT's observing time. More detailed information about these programs, designated 7226, 7227, and 7233 by the Space Telescope Science Institute (STScI), may be obtained through their Web server[d].

The 7226 candidate list contains 43 very young main-sequence stars with mean distances of ≤30pc. The median age for the candidates with well-established ages is ≤ approximately 90 Myrs and contains at least 6 candidates with ages as young as ≤ approximately 10 Myrs. Because of the extreme youth of these objects any low-mass brown dwarf and planetary companions will still be in a higher luminosity phase and thus easily detectable. For example, in it's first 10 Myrs a 10 M(Jupiter) brown dwarf would have a luminosity exceeding 10^{-4} L(sun)[7]. Given the NICMOS coronagraphic performance, as assessed in SMOV, we will be able to detect 3 M(Jupiter) companions near the inner radius of the search space in the ~25-minute integration time per candidate used in that program. We note that typical separations observable with NICMOS are near the empirical maximum in the binary distribution of stars (< approximately 20-40 AU), which also corresponds to the mean distance of the giant planets in our own solar system.

The 7227 candidate list contains 31 M-dwarf stars which are (a) nearby (distance < 6pc) with spectral types later than ~M3.5, (b) young (age < 100 Myr) with distances < 25pc, and (c) spectrally the latest known (i.e.,"ultra-cool" stars later than < M8.5), with some overlaps. Because of the proximity of many of the stars in this sample to the sun, companions as close as 1.2 AU from their primaries may be detected at the inner radius of our search space.

The 7233 candidate list contains 17 primarily main-sequence stars, with IRAS infra-red excesses, τ(dust) > 3, and other physical characteristics which may be indicative of the presence of circumstellar dust disks. For the brighter stars multispectral imaging will be carried out in narrower bandpasses including 1.71μm (HCO_2 + C_2 continuum), and 2.04μm (methane band), and in the line spectra of Paschen-α (1.87μm) and Bracket-γ (2.15μm)

The success of these programs will lie in the ability to repeatably reach the detection limits found achievable in SMOV. To do so care must be taken in the on-orbit operation of the instrument and in the details of the construction of the observing plan. Many of the most significant considerations for NICMOS coronagraphic operations are discussed in the subsequent sections of this paper.

---

[d] http://presto.stsci.edu/public/propinfo.html

3. THE NICMOS CORONAGRAPH - PHYSICAL DESCRIPTION

The design, fabrication, and incorporation of a coronagraph into NICMOS camera 2 optical system[8] allows us to push our investigations into previously and other-wise unreachable corners of the observational parameter spaces associated with the close environments of stars. The NICMOS-3 detector[9] (256x256 HgCdTe photo-diode array of 40μm square pixels, indium bump-bonded to a sapphire substrate) in camera 2 provides a 19.1"x19.2" field-of-view, with an image scale of ~0.076"/pixel. Diffraction limited performance is achieved to ~ 1.75μm. A coronagraphic spot re-imaged onto the focal plane results in a circular occulted region ~0.3" in radius.

The sizing of the coronagraphic hole (and, hence, it's angular extent projected onto the detector focal plane) was a natural consequence of optimizing the design of the coronagraph for H-band imaging. At a 300 milli-arcsecond annular zone, in an idealized point spread function, a natural break occurs in the encircled energy profile at 1.6 μm. At this wavelength (where the combined zodiacal and thermal backgrounds presented to NICMOS is at a minimum) ~93% of the energy in an idealized PSF is contained within a 300 milli-arcsecond radius of the center of the core. Radially outward from this zone the encircled energy profile essentially flattens out toward larger radii. (See Figure 1).

FIGURE 1

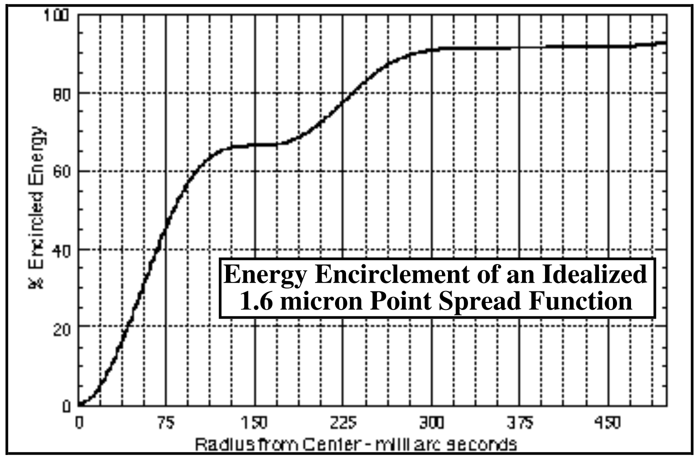

The NICMOS coronagraph is primarily comprised of two optical elements (Figure 2), exclusive of optical baffles. A 170-micron (physical diameter) hole has been laser ablated out of the C2 mirror in the NICMOS Field Divider Assembly (FDA), which is positioned at the Optical Telescope Assembly (OTA) f/24 image plane. The peaked-up centroid of the object Point Spread Function is placed at the center of the coronagraphic hole by an autonomous target location/acquisition process. Small irregularities within a 10-micron annulus at the "edge" of the hole (within allowable manufacturing tolerance) may be the principle source of residual scattered light at this radial region.

An oversized cryogenic pupil-plane mask (Lyot stop), maintained in-flight at ~100K, screens out residual radiation not only from the from the HST OTA primary and secondary mirror edges, but from mirror support structures (pads, spider, mounts, etc.) as well. The mask, with an obscuration area of approximately 85 percent, is located in the dewar's Vapor Cooled Shield, immediately ahead of the camera 2 filter wheel assembly.

FIGURE 2

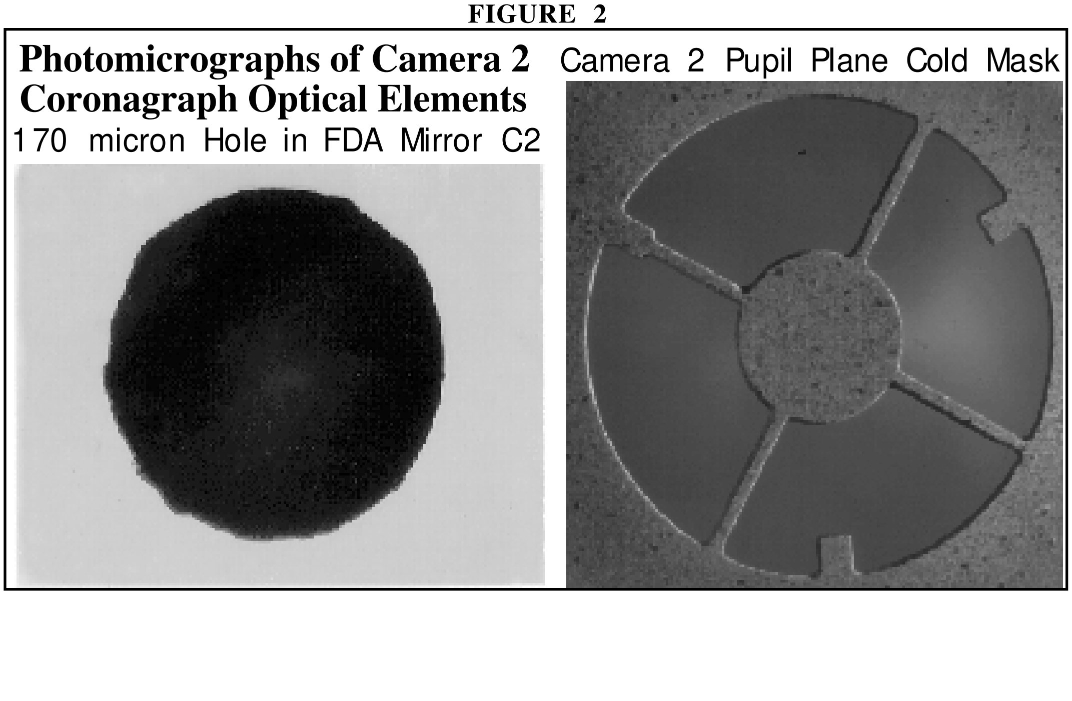

4. ON-BOARD AUTONOMOUS (MODE-2) TARGET ACQUISITION

The angular size of the occulting spot is on the order of, or smaller than, typical HST blind-pointing errors due to the absolute precision of the stellar coordinates in the Guide Star catalog. Therefore, the NICMOS flight software includes an autonomous Target Acquisition mode to remove the differential error in pre-planned target and Guide Star positions.

Coronagraphic target acquisitions are requested through STScI's proposal interface as acquisition mode exposures using a special aperture as described in the NICMOS Proposal Instructions[10]. In this process, after pointing to the field and acquiring Guide Stars, two images of the target are taken (for cosmic ray removal), and the brightest object in a 128x128 pixel "sub-array" in the coronagraphic acquisition aperture is located (Figure 3 - left). NICMOS will then request a vehicle slew whereby HST's pointing control system will move the spacecraft to place this object in the center of the occulting spot. Representative target acquisition images, obtained during the SMOV test program, are shown in Figure 4.

FIGURE 3

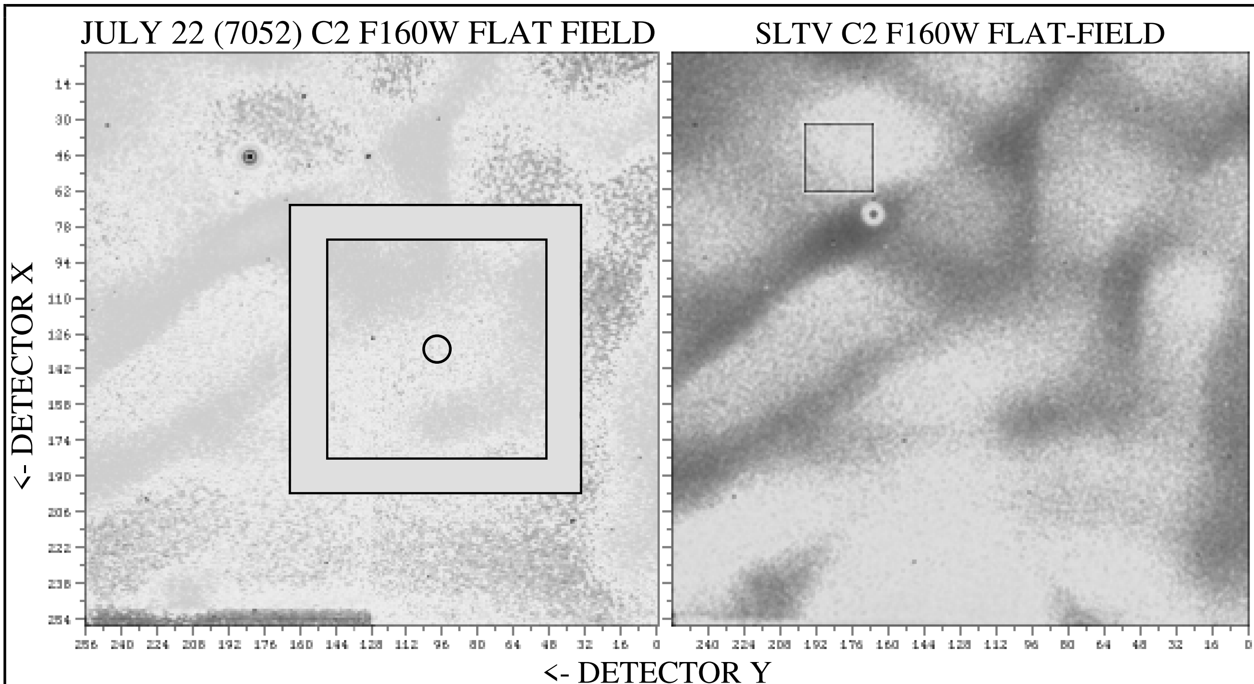

LEFT: The acquisition aperture (larger of the nested squares) is overlaid on internal flat field image. The circle, whose diameter is a typical "worst-case" blind-pointing error due to positional uncertainties in HST guide stars (~1"), indicates the aperture center. Targets cannot be reliably placed in the hatched region for this reason, making the effective reliable size of the acquisition aperture ~7.2" on a side. The dark circle at the upper left is due to the coronagraphic hole.

RIGHT: When locating the position of the coronagraphic hole a flat-field must be applied which does not contain an image of the hole. For this purpose a "gain table" taken from an inverted ground flat is used. During ground testing the gravity sag on the fore-optics bracket deflected the position of the hole as re-imaged on the detector.

The sublimation of the Nitrogen ice in the NICMOS dewar causes small positional shifts of the Camera 2 detector with time. This results in sub-pixel changes in the re-imaged projection of the coronagraphic hole at the detector f/45 focal plane on multi-orbit time scales. In order to maintain high-precision (better than 1/4 pixel) target centration the target acquisition process has been augmented to autonomously re-determine the position of the coronagraphic hole prior to acquiring a target. This process entails taking two pairs (for cosmic ray elimination) of F160W internal flat field exposures (and matching pointed backgrounds) to produce an image of the coronagraphic hole. This image is flat-fielded (Figure 3 - right) and a centroid determined with a weighted-moment algorithm. The updated hole centroid, with a "scatter point offset", to peak-up performance due to asymmetries in the system which were calibrated in SMOV, is used determining the slew offset maneuver which places the target in the coronagraphic hole. In principle this need be invoked only on multi-orbit time scales, but STScI has "packaged" this capability for simplicity of use, and it is done prior to every target acquisition.

FIGURE 4

TARGET ACQUISITION IMAGES

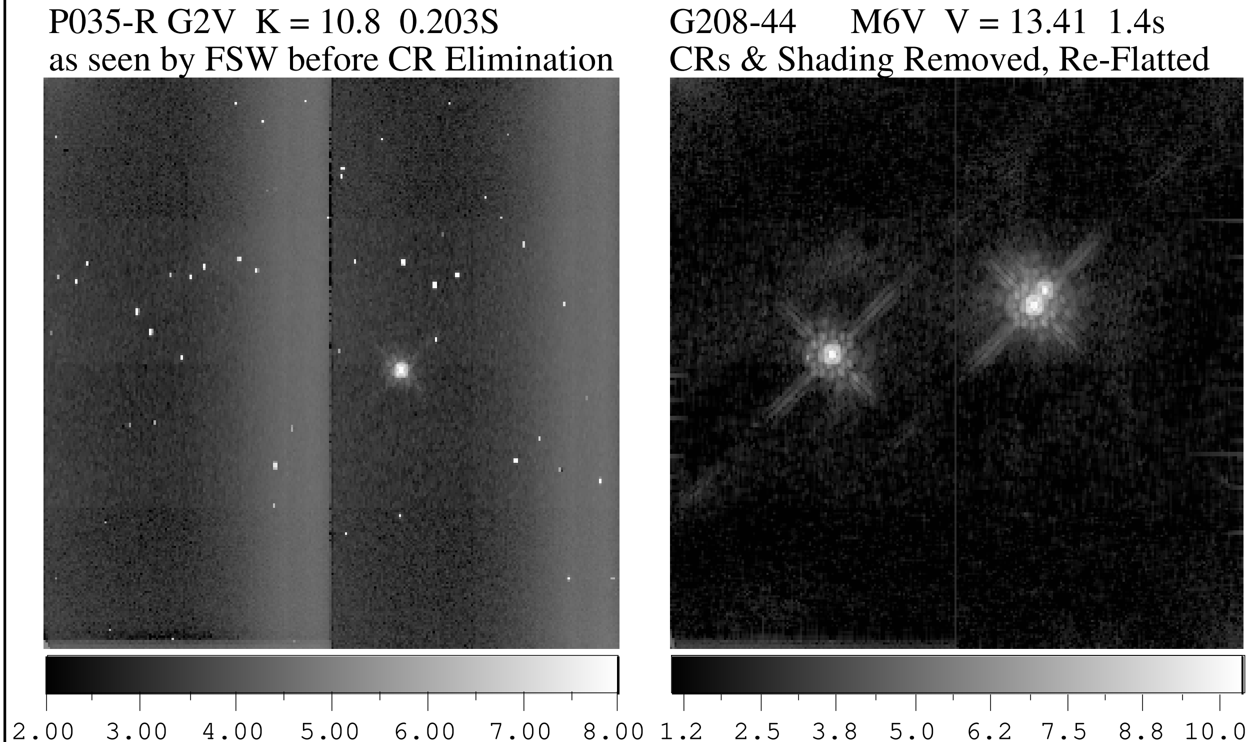

Flux units: ln(ADU) {+200 for P035-R}

Target Acquisition images from SMOV/7052 were obtained to demonstrate the ability to accurately acquire a variety of targets into the coronagraphic hole. The single star P035-R (left) was intentionally underexposed (note the strong shading gradient) to test acquisition in the low flux regime. In a more complex field the primary component of the close triple G208-44 was correctly located and positioned from on-board processing of the acquisition frames.

5. GROUND ASSISTED (MODE-1) TARGET ACQUISITION

Targets brighter than H < 3.6 will saturate in the core of their point spread functions at the shortest possible integration time with the narrowest (1% band-pass) filters. In such cases the on-board software will be unable to obtain an accurate target centroid. The NICMOS IDT has worked with the OPUS group at STScI to develop algorithms and procedures to allow acquiring brighter targets via near real-time analysis of downlinked acquisition frames. The capability to centroid on core-saturated PSFs now exists in OPUS and may be used for such targets.

The "Mode-1" process involves taking acquisition and calibration data to the ground in real-time, finding the core-saturated centroid, and uplinking a pointing correction to the spacecraft to be used in a "reuse target offset" slew. This process requires an additional orbit of spacecraft time as well as real-time communication with HST, and hence is a demanding resource. The limitations on Mode 1 and 2 target acquisitions are summarized in Table 1.

TABLE 1 - REGIMES OF TARGET ACQUISITION

1) Minimum Integration Time for ACQ Mode = 0.202s (specified as 0.237s via STScI's RPS-2 front-end).
2) Minimum Target Flux ~4230e- (~800 ADU above bias) for success.
3) For Targets Brighter Than H = 3.6 Must Use MODE-1 Target Acquisition.
4) For Targets 3.6 < H < 5.6 Offset pointing by (+1", +1") to move diffraction spike off Coronagraphic Hole (To Obtain an Unbiased Position of the Coronagraphic Hole).
5) "Optimum" Target Acquisition Integration: <2.5% Deviation from Linearity (162,000 e^-), Reduce by 30% for On-Board Flat-Fielding and Target Flux Uncertainty.

6. CORONAGRAPHIC FOCUS

By design, the image planes formed at the NICMOS FDA (which contains the coronagraphic hole at the OTA f/24 focus) and at the detector (reimaged through the NICMOS camera 2 f/45 stage-2 optics) are confocal. Because of the displacement of the cold well, arising from the expansion of the solid Nitrogen cryogen, the detector has moved forward from it's pre-launch design position. For direct imaging an internal refocus mechanism, ahead of the FDA, is used to refocus the f/45 beam on the detector. This, however, places the f/24 OTA focus ahead of the plane containing the coronagraphic hole. As a result, energy from a now afocal PSF core "spills out" of the coronagraphic hole thereby significantly reducing the local contrast ratios near the hole (due to both increased scattering and less effective diffractive energy rejection) as shown in Figure 5.

FIGURE 5

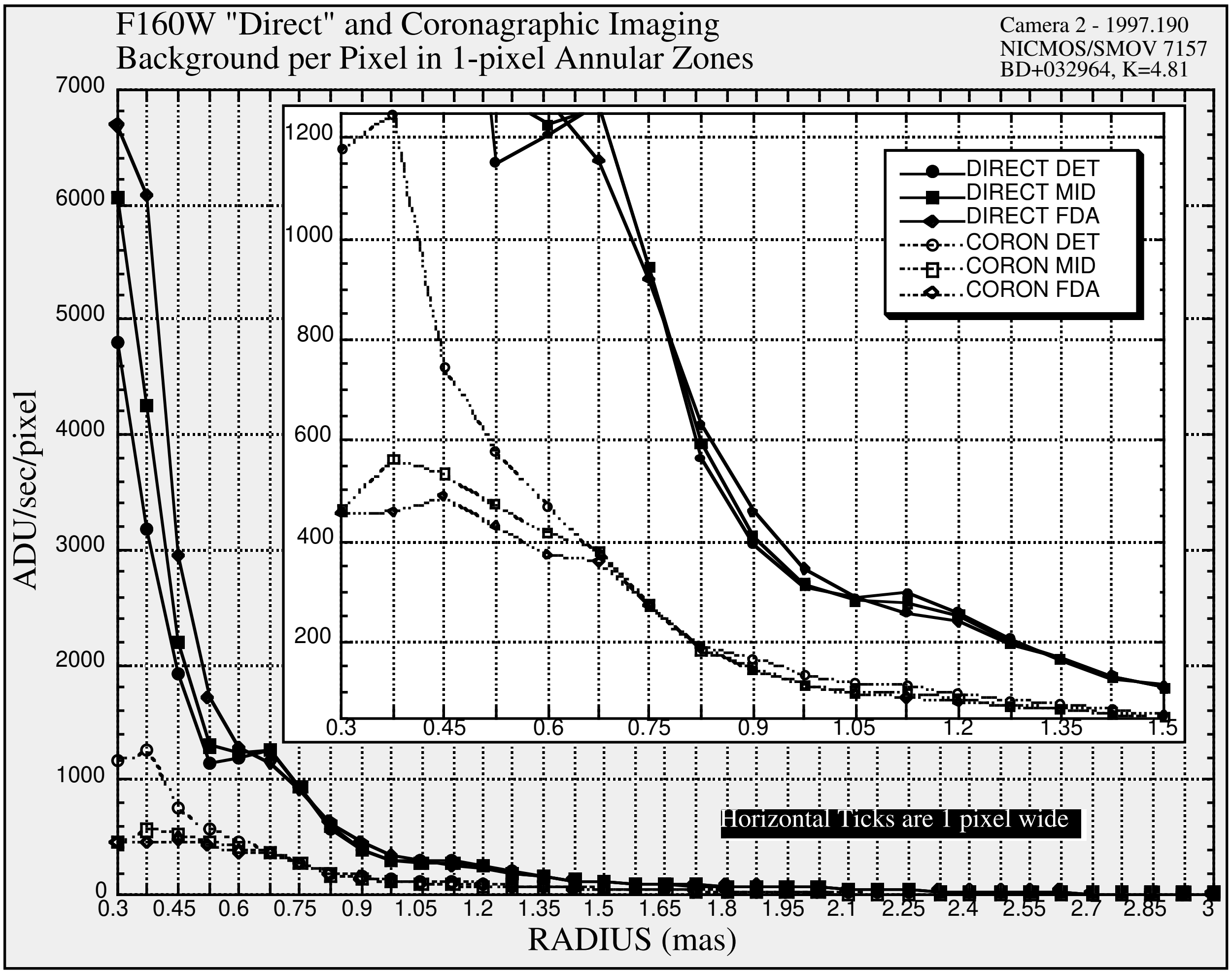

To restore the desired performance of the coronagraph the Pupil Alignment Mechanism (PAM) is used to automatically refocus the f/24 beam on the field divider mirror. As demonstrated in SMOV a displacement of the mirror in PAM space of ~2.6mm will peak up the performance of the coronagraph.

The substantial decrease in background near the hole is at the small, though very acceptable, expense of degradation in image focus quality at the detector. In the bandpass of the F160W filter this degree of defocus does not exceed the allowable $\lambda/14$ wavefront error, and decreases the flux in the peak pixel of a non-occulted stellar PSF by only ~4% (see figure 6). In contrast, the decrease in background by containment of the wings of the occulted PSF in the coronagraphic hole is improved by a factor of 2 to 3 near the hole. There is some color dependency[11] in both effects, as the smaller PSF at shorter wavelengths is better contained in the hole, but will have correspondingly larger wavefront errors for non-occulted targets which approximately scale with wavelength. Overall, however, the pre-launch anticipated coronagraphic performance is almost fully restored.

FIGURE 6

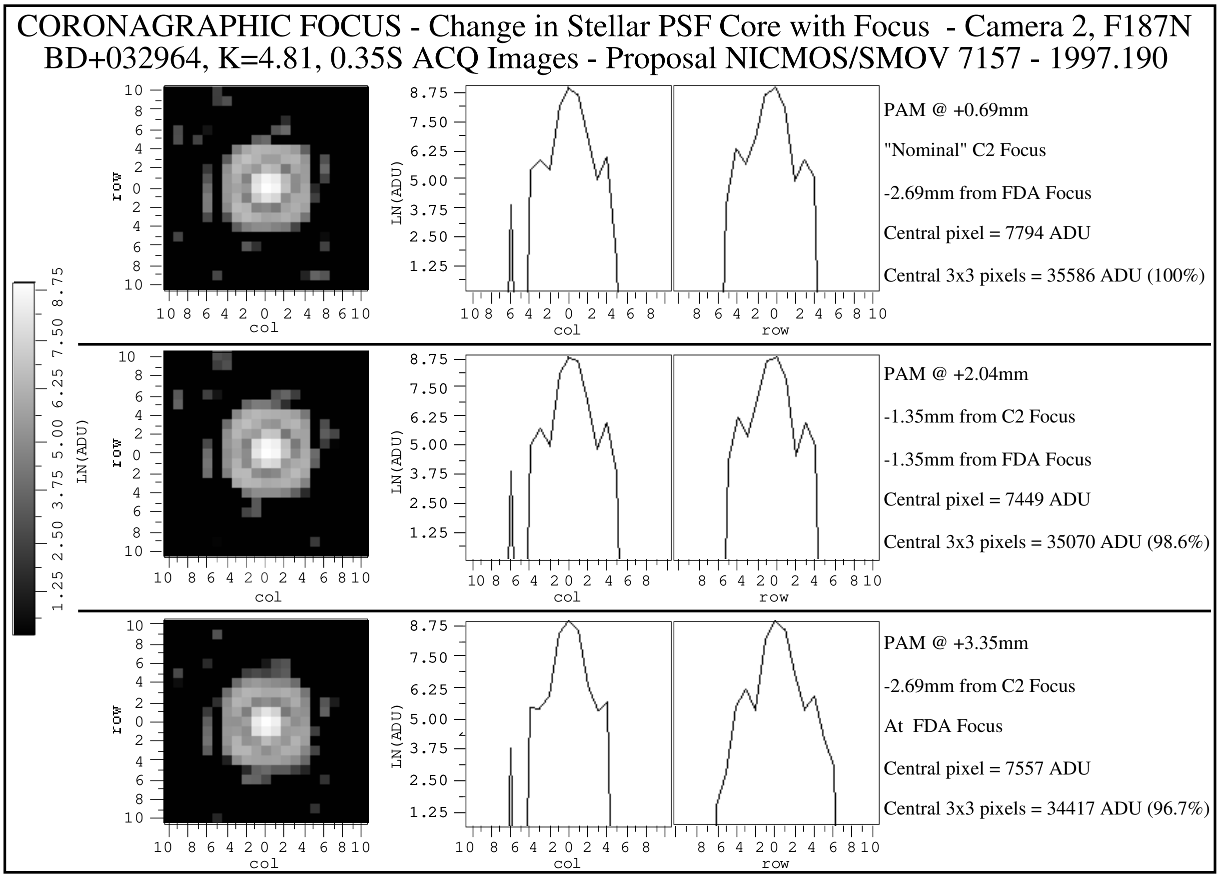

7. CORONAGRAPHIC PERFORMANCE

An aggressive 17-orbit commissioning, performance verification, and calibration program executed during SMOV allowed us to ascertain the true performance limits of the coronagraph[12] and optimize both it's operation and our observing programs. Performance profiles for NICMOS camera 2 direct, coronagraphic, and differential imaging derived from that test program are shown in Figure 7. We found that by subtracting coronagraphic PSFs at different spacecraft roll angles the background diffracted and scattered energy in the unocculted PSF-wings of an occulted primary star can be reduced to approximately one-millionth the peak intensity of the star at a radial distance of 1", or about 10^{-5} at 0.5. This is an improvement of more than two orders of magnitude over the already low backgrounds afforded by the diffraction-limited, highly stable, PSF. This represents a very significant gain over the current generation of AO ground-based coronagraphs[13] and is unique to NICMOS+HST.

The NICMOS coronagraph offers significant reductions in azimuthally averaged background energy from an occulted source in comparison to a direct image. In the bandpass of the F160W filter, at distances of 0.4"-0.7" from the center of the coronagraphic hole the background is reduced, on average, by a factor of ~6 (with greater reductions close in); from 0.7" to 1.4" by a factor of ~4; and from 1.4" to 3" by declining factors of ~3 to ~2.5.

Additional rejection in the azimuthally averaged background from subtracting two coronagraphic PSFs at different S/C roll angles increases from a factor of ~30 at the edge of the hole to more than 100 out to ~3.5". The product of these two effects yield reductions in background energy by factors on the order of one to several hundred over a single direct image. When used in this manner the coronagraph provides a gain of 5-6 magnitudes when trying to detect faint objects (or structures) near bright ones over direct imaging. The inset in Figure 7 compares azimuthally averaged backgrounds from the PSF wings in a direct image, a coronagraphic image, and by subtraction of coronagraphic images under the F160W filter.

FIGURE 7

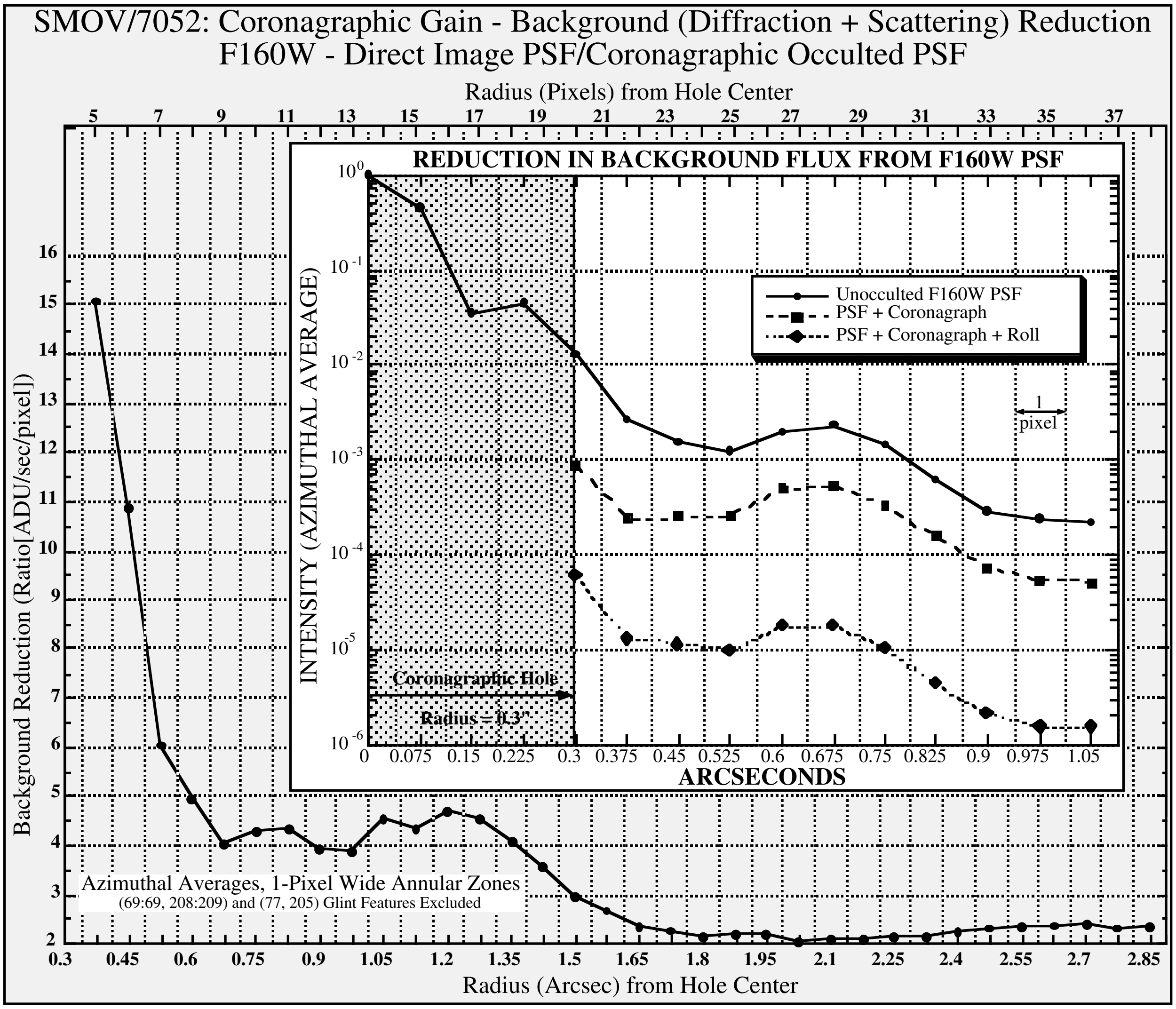

The efficacy of reducing the background light from an occulted stellar PSF by coronagraphic imaging is demonstrated in Figure 8. A non-coronagraphic image of a point source exposed to saturation to a radius of ~5 pixels in the core is shown on the left. An otherwise identical coronagraphic image is shown in the middle. The residual background from subtracting two coronagraphic images taken at S/C orientations differing by 35° is shown on the right.

In addition to the obvious relative increase in background in the direction of the OTA spider (along the diagonals), and in the speckle pattern of the inner coronagraphic PSF, two highly localized "glint" features appear near the edge of the coronagraphic hole. These may be seen, for example, in the central bottom panel in Figure 8. The photon noise associated with these features results in elevated residuals in the PSF subtraction of two coronagraphic images taken at different rolls, but are otherwise identical. Eg., note the two "bright spots" near the center of the PSF subtraction in the upper right panel of Figure 8. At these specific locations in the PSF the detection limits may be raised (degraded) by as much as ~2 magnitudes. This is discussed in the previously referenced SMOV test report.

A two-dimensional map of the region around the coronagraphic hole, illustrating the spatial characteristics of the background flux reductions achievable by coronagraphic PSF subtraction from images taken at different spacecraft orientations, is shown in Figure 9. The isophotes of flux reduction factors are in comparison to a coronagraphic PSF (not a direct image). The residual flux in the direction of the OTA diffraction spikes is typically higher by factors of 2-4 then at inter-spaced azimuthal directions (at the same radial distances). In planning observations, if one has a priori knowledge spatial orientation of the features of interest be imaged the telescope roll should be constrained not to place those features of interest along the diffraction spikes.

FIGURE 8

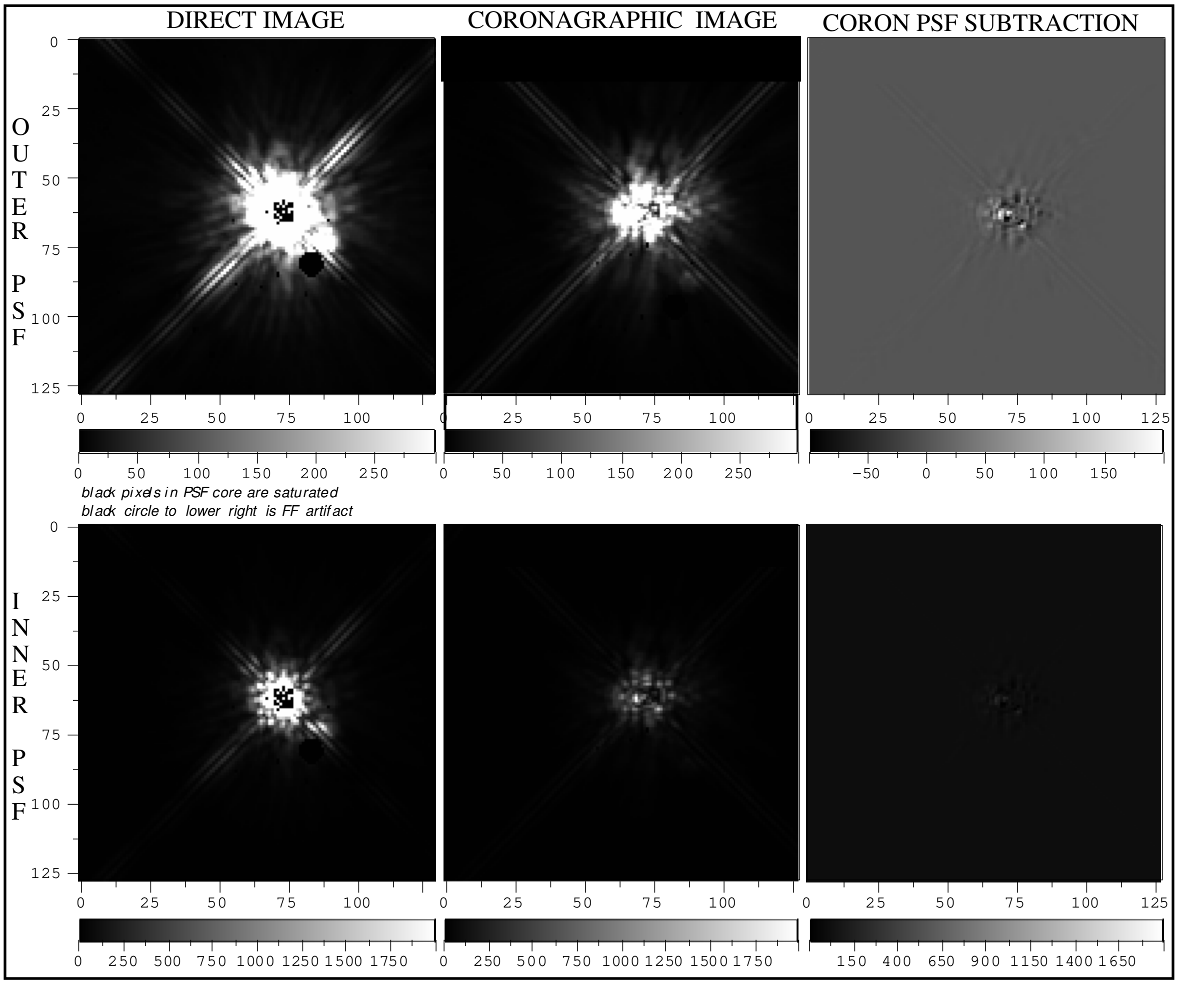

FIGURE 9

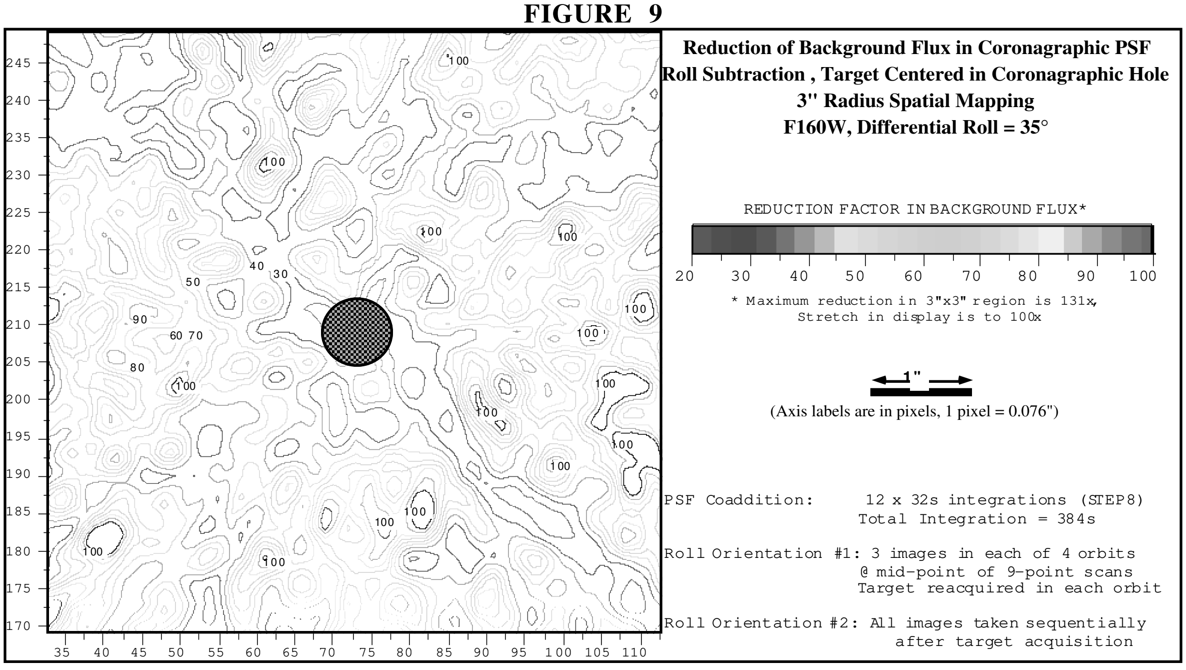

8. PSF STABILITY - "BREATHING" AND TARGET DECENTRATION

To achieve the levels of performance resulting from coronagraphic image subtraction as discussed in section 7, the stability of the PSF is paramount. The differential background arising from the subtraction of the unocculted wings of the occulted stellar PSF, from images at two different orientations, is dependent upon the ability of the Pointing Control System and on-board Target Location/Centration software to reposition the target in the coronagraphic hole after performing a roll maneuver. The error budget for the Target Acquisition process allows for a retargeting error of no greater than ±0.25 pixels. The effect on the background due to target decentration error (intentionally introduced) at these extremes and beyond was measured during SMOV. With concentric images the residual background near the coronagraphic hole, after image-pair subtraction, is only ~2% of the background in a coronagraphic PSF. Decentering the images by 0.25 pixels can result, locally, in increases in background (and reduction in contrast) by factors of 4 or more (see Figure 10). With a well-calibrated and fixed focal plane metrology the error budget is more easily met (also as demonstrated in SMOV). The need to ascertain the position of the coronagraphic hole by on-board S/W due to positional drifts of this magnitude on multi-orbit timescales would not introduce a differential targeting error for sub-orbit timescale dual-orientation observations. However, the "packaging" of the hole-finding process (by ground sequencing, not flight software) with every target acquisition may induce such differential errors due to random errors in determining the flux-weighted centroids of independent sets of hole-flats. The non-repeatability of the hole-finding process due to photon and systematic noise components will have to be assessed after a statistically significant number of augmented target acquisitions have been attempted on-orbit.

FIGURE 10

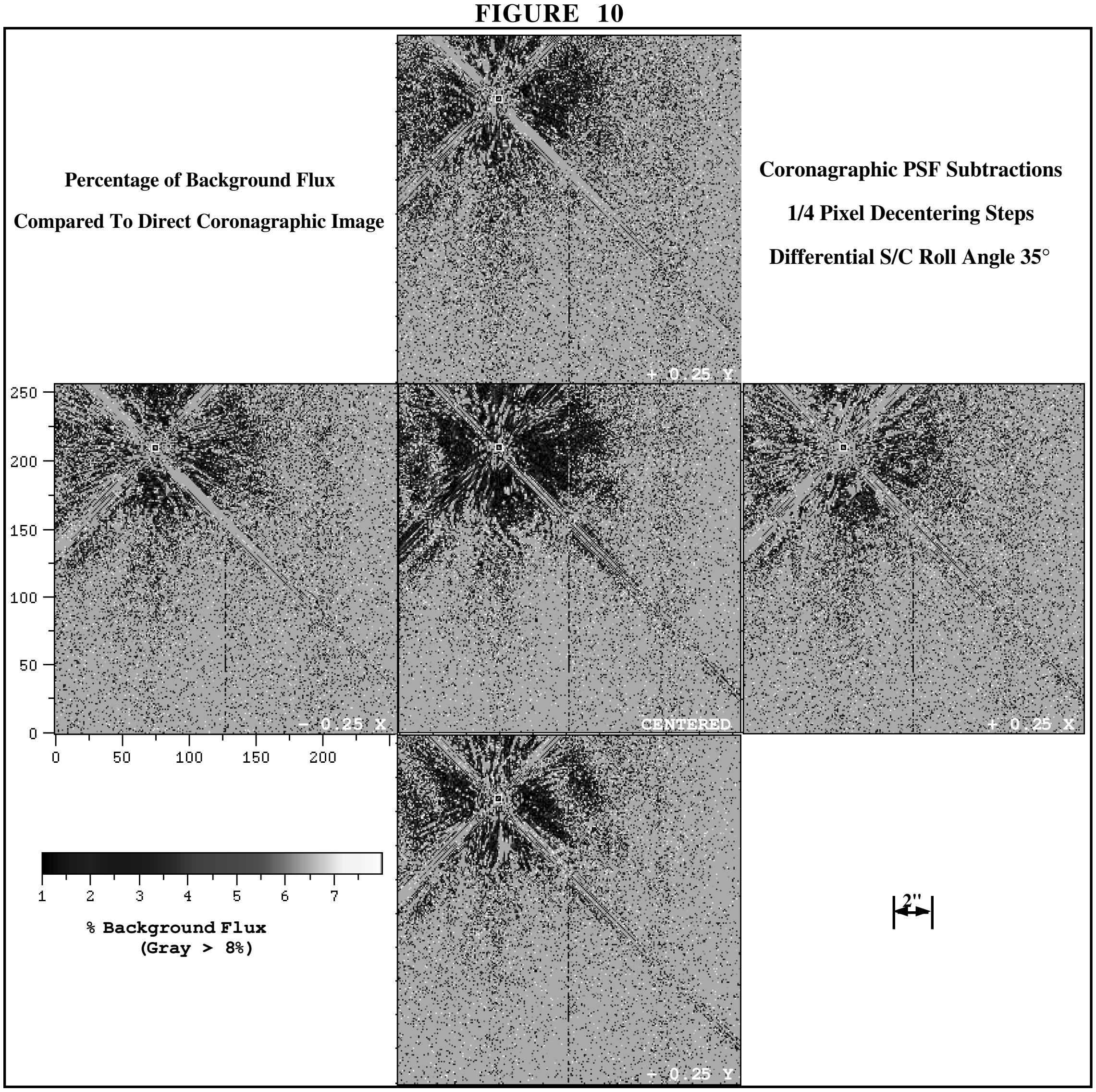

For the NICMOS GTO program observations at two spacecraft orientations are taken with no intervening Earth occultations or vehicle attitude changes to minimize the effects of OTA "breathing". Typical changes in the focal length of the OTA with variations in such thermal input as described by Hershey[14], would result in changes in focus at the Camera 2 detector of ~±0.7mm. Differential structure in the PSF with such changes in focus reduces the efficacy of PSF subtraction in the inner ~1.5" radius of the PSF by a factor of ~5 (see Figure 11). Programs which obtain images where the thermal inputs to the OTA have varied (due to interruptions in scheduling with interleaved attitude changes or Earth occultations) are subject to degraded performance in PSF subtraction. This situation is not unique to coronagraphic imaging, but due to the import of PSF subtraction to achieve the requisite performance levels this is a very significant issue. Figure 9 shows the anticipated increase in background from imperfect PSF subtraction due to typical multi-orbit time-scale breathing effects.

FIGURE 11

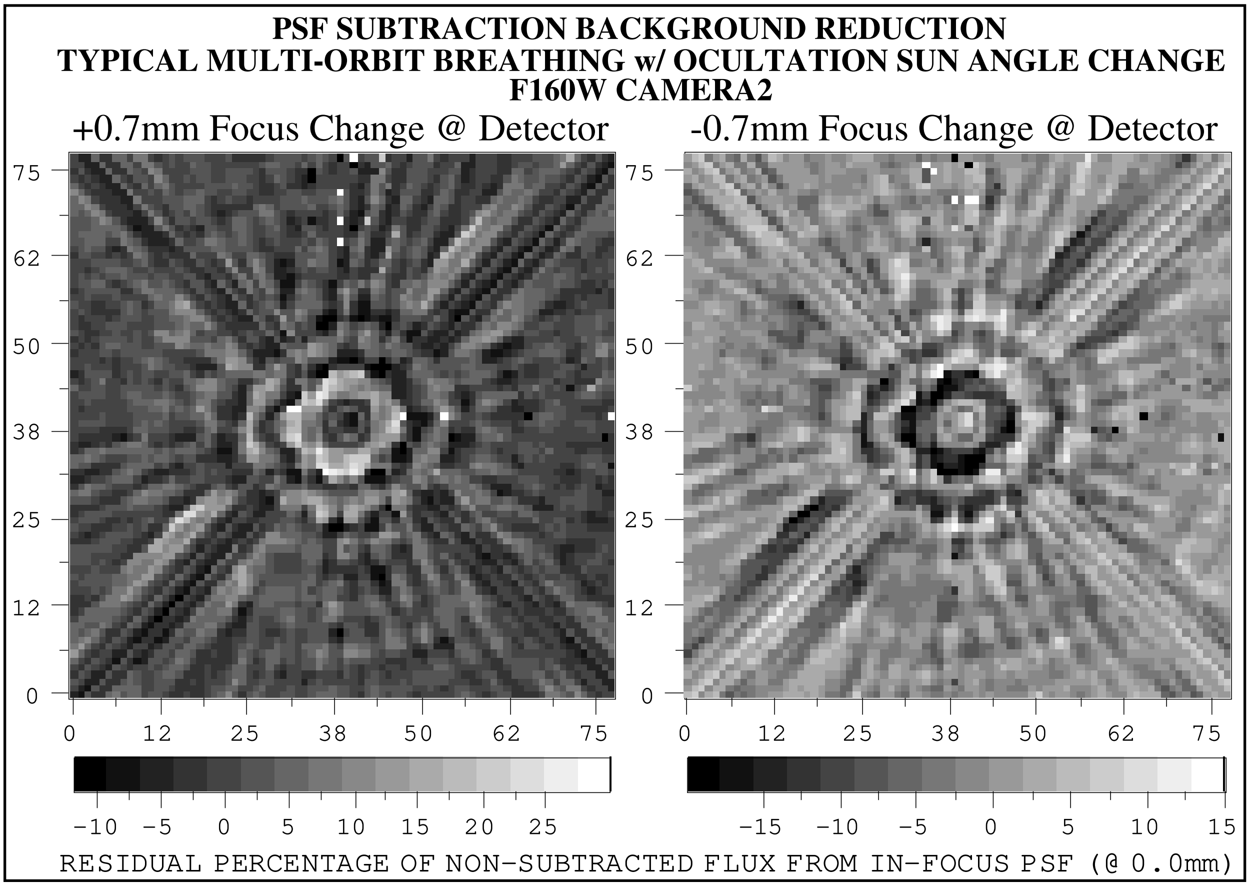

9. SUMMARY

The NICMOS coronagraph provides a powerful new tool to aid in the exploration of the environments of nearby stars. As demonstrated in substantial on-orbit testing, the performance levels achievable by the coronagraphic system meet or exceed the scientific requirements of the EONS search programs. Those programs, discussed in sections 1 and 2, are just commencing coincident with the issuance of this paper. Their success hinges upon routinely and repeatedly reaching the performance levels which have been reported here. Controlling the time-variable systematic errors which can degrade the coronagraphic performance will be difficult and will require a continuing commitment to on-going monitoring, calibration, and operations updates by the NICMOS IDT and STScI. With that commitment we look forward to reporting the scientific results of these programs at a future, but relatively near-term, epoch.

10. ACKNOWLEDGEMENTS

The design, fabrication, implementation, testing, and commissioning of the NICMOS coronagraphic system was possible only through the efforts of many people who contributed at many levels. We would like to thank the members of the NICMOS Optics, Integration and Test, and Flight S/W integrated product teams at Ball Aerospace Technology Corporation for their understanding and attention to detail in the construction of the instrument. The insights, input, and independent review of many aspects of optical issues by J. E. Mentzell, former NICMOS optical engineer at UofA (now at GSFC), have been greatly appreciated. Our gratitude is also extended to the many individuals at STScI and GSFC Codes 440 and 512 for their assistance in defining and developing in-flight operations and implementation of our scientific programs. In addition we would like to acknowledge the work of Patrick Lowrence, Davy Kirkpatrick, David Koehner, Roland Meyer and Dean Hines in the SMOV test program and in developing our observing programs.

This work is supported by the National Aeronautics and Space Administration under NASA grant NAG-5-3042.

11. REFERENCES

1. Dressler, A., *HST and Beyond: Exploration and the Search for Origins*, AURA Inc., Washington, Inc., inclusive, 1996.

2. Mayor, M. and Queloz, D., "A Jupiter-Mass Companion to a Solar-Type Star", Nature, 378, 355-359, 1995.

3. Butler, R. and Marcy, G., "A Planet Orbiting 47 Ursae Majoris", ApJ, 464, pp. L153-L156, 1996.

4. Marcy, G.W. and Buttler, R., "A Planetary Companion to 70 Virginis", ApJ, 464, pp. L147-L151, 1996.

5. Oppenheimer, B., Kulkarni, S., Matthews, K., Nakajima, T., "Infrared Spectrum of the Cool Brown Dwarf GL 229B", Science, 270, pp. 1478-1479, 1995.

6. Burrows, A, Hubbard, W. Lunine, J., Marley, M., Huillot T., Saumon, D., Friedman, R., "Extra-Solar Giant Planet and Brown Dwarf Models", *Planets Beyond The Solar System and Next Generation Space Missions*, D. Soderblom, ASP Conf. Series 119, pp. 9-17, ASP, San Francisco, CA, 1997.

7. Kulkarni, S., "Brown Dwarfs: A Possible Link Between Stars and Planets", Science, 276, 1350-1354, 1997.

8. Ramberg. E., "Optical design of NICMOS: the second-generation infrared instrument for the Hubble Space Telescope", *Space Astronomical Telescopes and Instruments II*, P. Bely and J. Breckinridge, Proc. SPIE Volume 1945, pp.383-389, 1993.

9. Shin, L., and Winters, G., "NICMOS Flight Focal Plane Assembly", *Space Astronomical Telescopes and Instruments II*, P. Bely and J. Breckinridge, Proc. SPIE Volume 1945, pp.371-382, 1993.

10. NICMOS Phase 2 Proposal Instructions, STScI, 1997.

11. Schneider, G., Smith, B., Terille, R., and Meyer, R. "Results from SMOV 7157, NICMOS Optimal Coronagraphic Focus Determination", http://nicmosis.as.arizona.edu/gschneid/7157/PS/, inclusive, 1997.

12. Schneider, G., and Lowrance, P, "Results from SMOV 7052 NICMOS Coronagraphic Performance Verification", http://nicmosis.as.arizona.edu/gschneid/7052/PS/, inclusive, 1997.

13. Sandler, D.,"The Potential for Direct Imaging of Extra-Solar Planets withGround Based Telescopes", *Planets Beyond The Solar System and Next Generation Space Missions*, D. Soderblom, ASP Conf. Series 119, pp. 175-190, ASP, San Francisco, CA, 1997.

14. Hershey, J., "Modeling HST Focal Length Variations", Space Telescope Science Institute Report SESD-9701, inclusive, 1997.